Outer-shell photodetachment of the metastable Mg⁻ [core]$3s3p^2$ and Ca⁻ [core]$4s4p^2$ $^4P^e$ states

José Luis Sanz-Vicario,[1,*] Juan Carlos Cardona,[1] and Eva Lindroth[2]

[1]*Sede de Investigación Universitaria (SIU), Instituto de Física, Universidad de Antioquia, Medellín, Colombia*
[2]*Atomic Physics, Fysikum, Stockholm University, S-106 91 Stockholm, Sweden*

We report on calculated outer-shell photodetachment cross sections from the metastable [core]$nsnp^2$ $^4P^e$ states in Mg⁻ ($n=3$) and Ca⁻ ($n=4$) negative ions in the photon energy range $\omega=0-10$ eV. Double-ionization thresholds for Mg II and Ca II as well as doubly excited thresholds of the residual atoms Mg I and Ca I are located within the photon energy range considered and thus doubly and triply excited states of both Mg⁻ and Ca⁻ are reached. We use a complex scaled configuration interaction (CSCI) method for the three active electrons supplemented with a sophisticated model potential as developed by Laughlin [Phys. Scr. **45**, 238 (1992)] to account for core-valence interactions. The CI calculations are based on Mg⁺ and Ca⁺ one-electron orbitals expanded in terms of B-spline basis set. We compare our cross sections with the only calculation available up to a photon energy 0.25 Ry ($\omega \sim 3.4$ eV) [Zeng *et al.*, Phys. Rev. A **62**, 022713 (2000)] performed by using the R-matrix method, in which only one $^4P^o$ resonance for Mg⁻ and two ($^4P^o$ and $^4D^o$) for Ca⁻ were predicted. In this work, by analyzing both the cross sections and the locations of the S-matrix poles in the complex plane, we are able to predict six $^4P^o$, four $^4D^o$, and four $^4S^o$ resonant states for Mg⁻, and three $^4P^o$ and two $^4D^o$ resonant states in Ca⁻.

PACS number(s): 32.80.Gc, 31.15.vj, 31.15.ac

I. INTRODUCTION

The study of negative atomic ions has become a center of attention for the atomic physics community and is the subject of several books and reviews [1–6]. Negative ions are characterized in their structure and dynamics as being strongly correlated, and their weak binding is almost entirely due to this electron correlation. Highly excited states in negative ions are usually described as a complicated mixing of correlated configurations and consequently they should manifest specific structures in photoionization spectra. At variance with two-electron atomic systems, for which a long theoretical experience has been accumulated through the years in the accurate computation of doubly excited states and related photoionization processes, three-electron atomic systems are a present matter of study. Despite the extraordinary development of computer technology, precise calculations for three-electron atomic systems represent still today the cutting edge of complete *ab initio* treatments, allowing for results with spectroscopic accuracy within a few meV.

Considerable attention has been paid in the last 20 years to discovering bound states in alkaline-earth negative ions, in both their doublets and quartets [5]. Within the latter spin group, [core]$nsnp^2$ $^4P^e$ and [core]np^3 $^4S^o$ metastable states for Be⁻ ($n=2$), Mg⁻ ($n=3$), and Ca⁻ ($n=4$) were already predicted theoretically in the 1980s [7]. In contrast to Be⁻, for which the existence of such states has been confirmed experimentally in a definite way [8–10], the situation has been quite controversial for Ca⁻ $^4P^e$ [11–13] and impossible for Mg⁻ $^4P^e$, due probably to its very short lifetime (<1 ns) (see [5] and references therein). Photodetachment from the Ca⁻ $^4P^e$ ground state has already been studied, both theoretically [14–17] and experimentally [13,18–20] but, surpris-

ingly, there is only one photodetachment R-matrix study for the spin quartets available [21]. The last paper also contributed to studies of Be⁻ and Mg⁻ $^4P^e$ photodetachment. Since we already reported a comprehensive study on Be⁻ $^4P^e$ photodetachment [22], and we also compared with Ref. [21], we deal only with Mg⁻ and Ca⁻ in this work.

Outer-shell photodetachment in Mg⁻ and Ca⁻ involves actively only the three valence electrons, which implies that computer codes developed for pure three-electron atomic systems can be readily adapted to more complex systems provided we separate the system into an inert core plus valence electrons. This amounts to including the core-valence interactions through model potentials in an approximate way. Analytical model potentials and pseudopotentials are widely used in many contexts and they have received a deal of attention in atomic physics as well [23,24], in such a way that there is a considerable assortment of models at our disposal to be tailored for the specific system at hand.

This work follows a series of recent papers by our group that studied resonant structures and photodetachment in He⁻ [25] and in Be⁻ [22,26] by means of a complex scaled configuration interaction (CSCI) approach, which has proven to be very successful and accurate. In the Be⁻ case, we already introduced the implementation of simple model potentials in our method of solution. In the present case, Mg⁻ and Ca⁻ ions are more involved to compute, even as a three-effective-electron system, due to the size and complexity of their polarizable core. Although valence correlation among the three outer electrons is properly accounted for with the configuration interaction approach, we must rely on more sophisticated model potentials for the core-valence interaction, like those developed by Laughlin [27,28]. This model potential was already applied with success to compute Ca I excited states [29] and the Ca⁻ ^2P ground state [30]. The application of this potential in Mg⁻ is straightforward. In contrast, in Ref. [29] a proposal was introduced for a modification to the

———————
*Corresponding author. sanjose@fisica.udea.edu.co

one-electron model potential for d orbitals, that turned out to be of the utmost importance to correctly describe Ca I terms with a marked d character. We make use not only of this d correction in our Ca$^-$ calculations but also of the dielectronic polarization terms among the valence electrons. In this way, our computation contains all the required state of the art ingredients to compute Mg$^-$ and Ca$^-$ resonance states and their photodetachment. In spite of that, we still face some limitations for a precise computation in Ca$^-$.

This paper is organized as follows. In Sec. II we introduce our method of solution with the construction of one-electron orbitals in terms of B-spline basis sets and the three-electron complex scaled configuration interaction approach with their supplementary corrections. In Sec. III we report our calculations and results for the characterization of Mg$^-$ and Ca$^-$ resonant states within the photon energy region considered ($\omega = 0-10$ eV) and their partial and total photodetachment spectra. We end up with some conclusions. Atomic units are used throughout unless otherwise stated.

II. THEORY

A more detailed account of our CSCI approach was presented in a previous work [25]. Major changes from this description are due to the inclusion of a sophisticated model potential in the solution of one-electron radial equations and the extra corrections in the interactions among the valence electrons, which are here described in detail. A further development over previous descriptions consists in the implementation of exterior complex scaling to assess the appropriate use of uniform complex scaling when such model potentials are in use.

A. One-electron orbitals: Model potential

The three-outer-electron problem is solved by expanding the total wave function in terms of configurations using a basis of one-electron orbitals $\phi_{nlm}(r,\Omega) = P_{nl}(r)/r\mathcal{Y}_{lm}(\Omega)$, which are obtained as eigenfunctions of a reduced radial equation for $P_{nl}(r)$:

$$\left(-\frac{1}{2}\frac{\partial^2}{\partial r^2} + \frac{\ell(\ell+1)}{2r^2} - \frac{Z}{r} + V_\ell^{\text{model}}(r) - \epsilon_{n\ell}\right)P_{n\ell}(r) = 0,$$

(1)

where Z is the nuclear charge and $V_\ell^{\text{model}}(r)$ stands for the potential that accounts for the core-electron interaction. These radial orbitals are then complex-rotated to enter the three-electron CSCI, as explained below.

The one-electron radial function $P_{nl}(r)$ is expanded in terms of N B-splines of polynomial order k confined in a box of length $[0, r_{\max}]$, where $r_{\max}$ is the box size. The B-splines are defined in a set of knot points distributed in a combined linear-exponential sequence. The use of B-splines implies a better description of diffuse wave functions that represent loosely bound (resonances) or continuum states in terms of relatively short expansions. A comprehensive report on the application of B-splines in atomic and molecular physics is available [31].

In Be$^-$, with a $1s^2$ core, polarization effects are less important and, accordingly, we used in Ref. [22] a simple model potential that sufficed to provide rather accurate one-electron orbitals and energies. Moving further into the series of alkaline-earth atoms, the core becomes more complex and, accordingly, so does the required model potential. There is a plethora of different atomic model potentials at our disposal in the literature that may be adapted specifically for alkaline-earth systems (see, for example, Albright *et al.* [32] and the review by Aymar *et al.* [33]). The appropriate selection depends on the atomic system itself, the type of process under study, and the required accuracy in the computed solution. In fact, effective model potentials regarded as accurate to compute some properties of metastable alkaline-earth atoms [34] are not indeed accurate when dealing with Ca$^-$ resonant structure and its photodetachment. Previous works on Ca$^-$ [30,35,37] and our present experience reveal that precise computations on alkaline-earth negative ions beyond Be$^-$ require an optimal choice of one-electron orbitals. The most sophisticated model potential to date has been developed by Laughlin in a series of papers [27,28], and reads

$$V_\ell^{\text{model}}(r) = \mathcal{V}_{\text{HF}}^d(r) + V_{\text{pol}}(r) + U_\ell(r).$$

(2)

The direct Hartree-Fock potential $\mathcal{V}_{\text{HF}}^d(r)$ has the form

$$\mathcal{V}_{\text{HF}}^d(r) = \sum_{n\ell}^{\text{core}} 2(2\ell+1)\int_0^\infty dr' \frac{1}{r_>}|P_{n\ell}^{\text{core}}(r')|^2,$$

(3)

where $r_> = \max(r,r')$ and the sum runs over the core wave functions $P_{n\ell}^{\text{core}}$, which we have extracted from the tables of Clementi and Roetti [38]. The above integral is evaluated within the B-spline knot-sequence grid through a double Gauss-Legendre quadrature. The polarization potential includes the dipole, α_d, and quadrupole, α_q, polarizabilities of the Mg$^-$ and Ca$^-$ cores,

$$V_{\text{pol}}(r) = -\frac{\alpha_d}{2r^4}W_6(r/r_c) - \frac{\alpha_q - 6\beta_1}{2r^6}W_8(r/r_c),$$

(4)

where β_1 is the first-order dynamical correction to the dipole polarizability α_d. The role of the cutoff functions $W_n(r) = 1 - \exp(-r^n)$ is to eliminate the short-range behavior of the polarization potential by suppressing its penetration into the core region $r < r_c$. The ℓ-dependent potential U_ℓ is expressed in the form

$$U_\ell(r) = (a_0^\ell + a_1^\ell r + a_2^\ell r^2)\exp(-a_3^\ell r),$$

(5)

where the four adjustable coefficients a_n^ℓ are determined by a least-squares fitting procedure with respect to the experimental Mg II and Ca II levels. We also choose to keep the parameters α_d, α_q, and r_c fixed.

Incidentally, a local exchange potential as developed by Furness and McCarthy [39] may be added to the model potential to approximately include exchange effects between the valence and the core electrons. In some cases, it has been proved to be useful [32], but in our experience, although the energies are notably improved over the HF (direct) ones (the exchange effect is rather important), the orbitals start to develop unwanted oscillations close to $r=0$ during the process of parameter optimization of the potential U_ℓ, so that we

avoid the use of local exchange potentials. Anyway, it is assumed that U_ℓ partially makes up for these core-valence exchange interactions as well as for most of the one-body relativistic corrections, since we adjust to the experimental energies. Two-body relativistic effects are not included explicitly in our calculation, but they were found in Ca [36,37] to be smaller than one-body corrections, the latter being around 7 meV.

B. The form of the complex scaling

In this work we use the uniform complex scaling (UCS) method, where the radial electron coordinate is *uniformly* complex-rotated ($r \rightarrow re^{i\theta}$) from $r=0$. This allows for the $\mathcal{L}^2$ integrability of the rotated continuum wave functions. We first adjust the model potential V_ℓ^{model} when the rotation angle is zero and then the complex rotation is applied normally. In our previous work on Be$^-$ [22] we used the direct approach procedure to UCS, i.e., the knot sequence for the B-splines was defined in the real axis, and the kinetic energy T and the pure Coulomb V terms in the Hamiltonian were computed in the real axis and were then complex-scaled as $e^{-2i\theta}T$ and $e^{-i\theta}V$, respectively. Only model potentials, which are nonlinear, were explicitly scaled. Instead, for the present study, we have modified our codes to allow for the integration of matrix elements in any arbitrary contour in the complex plane. With such modification we can now also use exterior complex scaling (ECS), where the rotation takes place only beyond a given radial distance r_0 [$r \rightarrow r_0 + (r-r_0)e^{i\theta}$]. When $r_0=0$ we recover again the UCS case. The ECS application implies the use of basis sets of complex B-splines defined in the ECS contour instead of real B-splines. ECS received its full glory in more recent scattering applications, given that this approach provides the remarkable property that exact asymptotic scattering boundary conditions are satisfied by the ECS wave function at r_0 (see [40] and references therein). This property is not directly used in our computations, in which we do not look specifically at ejected electrons.

Our interest in ECS was motivated instead by the nonlinear form and the complexity of the model potential used in this work. It is not proved that complex scaling has a universal application to any arbitrary potential in terms of dilatation analycity in the complex plane, which is mathematically a nontrivial issue. Even when a potential is formally dilatation analytical, and thus all high-order derivatives are defined, fast variations with respect to the radial coordinate might cause computational problems. This happens since the numerical performance is governed not only by the formal existence of higher derivatives, but also by the possibility to represent them numerically. A way round is to avoid the complex rotation in the region where the model potential is effective. In fact, it has been formally proved [41] that the complex eigenvalue spectrum of the Hamiltonian depends only on the transformation into complex coordinates in the asymptotic region. Since these model potentials have a short range, it amounts to using ECS with a selected r_0 outside the effective range of the potential just to get past any potential nonanalycities. This is one of the potential applications of
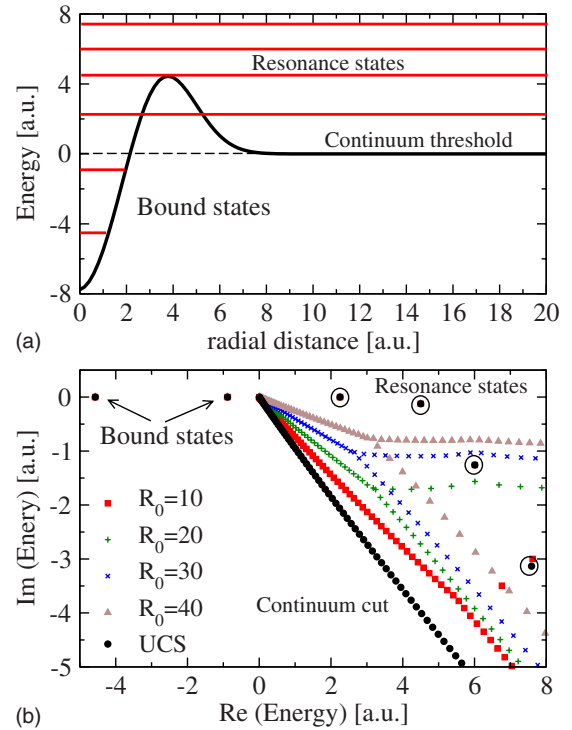

FIG. 1. (Color online) (a) Model potential given by Eq. (6) with energy positions of bound and resonant states above the continuum threshold. (b) Complex eigenvalue spectrum for this model potential computed with UCS with rotation angle $\theta=20°$ and several ECS computations with the same rotation angle and varying r_0.

ECS, already pointed out by the pioneers (see, for instance, Refs. [42,43]).

In practice, in computing resonance parameters and the photodetachment spectra of Be$^-$ using ECS with $r_0=5$ a.u. we find indeed an identical result as we obtained with UCS [22]. Similarly, it also happens in Mg$^-$ and Ca$^-$ with the present model potential of Eq. (2) with very slight changes due to the chosen r_0 value. Without being rigorous, this numerical equivalence shows in a phenomenological way that the application of UCS over such effective model potentials is appropriate. Although the UCS and ECS procedures are formally equivalent, in practical calculations with finite basis, they show a distinct behavior due to the presence of the extra parameter r_0. In order to illustrate this point we apply both UCS and ECS approaches to uncover resonance parameters in a toy one-electron model potential [44]:

$$V(r) = Ae^{-\alpha(r-a)^2} + Be^{-\beta r^2} \tag{6}$$

with $A=5$, $B=8$ $\alpha=0.25$, $\beta=0.2$, and $a=3.5$. This potential supports two bound states plus a series of shape resonances, as shown in Fig. 1. They are computed by solving the radial equation with a basis set of 300 B-splines (order $k=7$) distributed in a linear sequence of knot points within a box of 60 a.u. Also in Fig. 1 we plot the complex eigenvalue spectrum for a fixed rotation angle $\theta=20°$ and varying the r_0 value at which the ECS starts, including the case $r_0=0$ (UCS). By modifying only the parameter r_0 it is clear that the effective rotation departs from $\theta=20°$. For $r_0=10$ a.u., a dis-

tance that is outside the range of the potential, the ECS result slightly differs from the UCS one and the resonances are still correctly uncovered provided the resonance widths are not very large. In addition, for $r_0 > 0$, an unpleasant effect happens to occur in the ECS approach when using finite basis sets (see also [45]). The continuum cut splits into two branches and the upper new branch may hide the resonant states for large r_0 values. In addition, this upper branch eventually returns to the real axis at a higher energy. In the case of multichannel systems with several open thresholds, this latter effect may interfere in the visualization of higher resonances and the clear identification of the opening of successive thresholds. Fortunately, most of the resonances in Be⁻, Mg⁻, and Ca⁻ have small widths and lie very close to the real axis, and thus ECS and UCS will produce basically the same results in resonance parameters and the photoionization spectrum, although this may not be the general case. A comment in passing is now pertinent. When using complex *B*-splines in ECS a major problem on computing two-electron integrals was posed and a detailed algorithm then proposed [45]. In our approach, with the above-mentioned implementation of integration of one- and three-electron integrals for any complex contour, these bielectronic integrals may be computed accurately with a double Gauss-Legendre quadrature in the complex path, without requiring any special algorithm. In conclusion, we make use of the UCS approach to avoid any arbitrariness with r_0 in ECS once we have checked that the UCS applies safely with such model potential.

C. Three-electron system

The alkaline-earth negative ions may be described by the three-electron Hamiltonian

$$H = \sum_i h_i^{\text{model}} + \sum_{i<j} V(r_{ij}), \tag{7}$$

where the sums involve only the three outer-shell electrons and the expression for the model Hamiltonian h^{model} can be inferred from Eq. (1). The interaction term in Eq. (7) is

$$V(r_{ij}) = \frac{1}{r_{ij}} - \frac{\alpha_d}{r_i^2 r_j^2} \mathcal{P}_1(\cos\theta_{ij}) W_3(r_i/r_c) W_3(r_j/r_c)$$
$$- \frac{\alpha_q}{r_i^3 r_j^3} \mathcal{P}_2(\cos\theta_{ij}) W_4(r_i/r_c) W_4(r_j/r_c), \tag{8}$$

where $\mathcal{P}_n$ denotes a Legendre polynomial of degree n. The second term on the right side in Eq. (8) corresponds to a dielectronic dipole polarization potential and the third one to a quadrupole polarization potential [46,47], with their cutoff functions $W_n(r)$, as defined above. Both of them can be easily implemented by slightly modifying the routine for the two-electron integrals. These terms tend to reduce the binding effect and their inclusion has proven to be crucial to obtain accurate electron affinities in Ca⁻ [30].

Once the U_ℓ potential is fitted, the complex rotated eigenfunctions from Eq. (1) are then used to build three-electron configurations adapted to the total symmetries L, S and parity π. The matrix elements of the effective three-electron Hamiltonian of Eq. (7) are evaluated and the much bigger associated generalized complex symmetric eigenvalue problem is solved. With the three-electron eigenfunctions obtained, the photodetachment cross section as a function of the photon energy is calculated with the expression [48]

$$\sigma(\omega) = \frac{1}{2L_0+1} \frac{4\pi}{3} \frac{\omega}{c} \text{Im}\left(\sum_n^M \frac{\langle \tilde{\Psi}_0 | P | \tilde{\Psi}_n \rangle^2}{\tilde{E}_n - E_0 - \hbar\omega} \right), \tag{9}$$

where $\tilde{\Psi}_0$ denotes the initial state wave function with an energy E_0, $\tilde{\Psi}_n$ corresponds to the final states with complex energy $\tilde{E}_n$, let them be bound, resonant, or continuum states and $\tilde{\mathbf{P}} = \Sigma_{i,q} r_i' e^{i\theta} \mathbf{C}_i^{(q)}$ is the rotated dipolar operator in the length form. Because of the presence of the polarizable core the radial part in the dipolar operator is also modified [49–51] as follows:

$$r_i' = r_i \left(1 - \frac{\alpha_d}{r_i^3} W_3(r_i/r_c) \right). \tag{10}$$

III. RESULTS AND DISCUSSION

The initial state considered for Mg⁻ and Ca⁻ has the form $[\text{core}]nsnp^2 \, {}^4P^e$ with $n=3$ for Mg⁻ and $n=4$ for Ca⁻ and the final states after photon absorption correspond to ${}^4P^o$, ${}^4D^e$, and ${}^4S^o$ symmetries. Thus, the photodetachment process for $A^- \, (A=\text{Mg}, \text{Ca})$ reads

$$A^-([\text{core}]nsnp^2 \, {}^4P^e) + \omega \rightarrow \sum_{{}^4L^o} \{A([\text{core}]n'\ell'n''\ell'') \, {}^3\tilde{L}^\pi$$
$$+ e^-(\epsilon\ell)\} \, {}^4L^o, \tag{11}$$

where ω denotes the photon and ϵ corresponds to the energy of the detached photoelectron. For instance, within the photon energy range considered in this work, from 0 to 10 eV, the label $n'\ell'$ in Eq. (11) represents Mg I $3s$ and $3p$ orbitals only, and $n''\ell''$ may reach up to $n''=7$ since the thresholds Mg $[\text{core}]3s7d \, {}^3D$ at ~5.0 eV and Mg $[\text{core}]3p7s \, {}^3P^o$ at ~9.2 eV are reached. Note also that double-ionization thresholds Mg⁺ ${}^2S^e$ and Mg⁺ ${}^2P^o$ lie within this photon energy range at ~5.25 eV and ~9.68 eV, respectively. Similarly in Ca⁻, at least the double-ionization thresholds Ca⁺ ${}^2S^e$ at ~4.74 eV, Ca⁺ ${}^2D^e$ at ~6.4 eV, and Ca⁺ ${}^2P^o$ at ~7.86 eV are inside this region. Therefore, double photodetachment channels should be rigorously included and in our CSCI method they are, at variance with *R*-matrix methods.

We first solve the one-electron eigenvalue problem of Eq. (1) for the Mg⁺ and Ca⁺ ($[\text{core}]n\ell$) states with a basis set of 22 *B*-splines of order $k=7$, and a box length of 100 a.u. for Mg⁺ and 60 a.u. for Ca⁺. Our basis of *B*-splines is reduced to 22 (and also the one-electron orbitals) to prevent the number of three-electron configurations from being too large ($>10\,000$). This forces us to find the best representation of both bound and continuum states in terms of a reduced but well-tempered basis of orbitals. Orbitals expanded with *B*-splines provide such an optimal representation [31]. Parameters for the polarization potential $V_{\text{pol}}(r)$ in Eq. (4) were taken from Ref. [27] for Mg⁺ and from Ref. [52] for Ca⁺, and

TABLE I. Model potential parameters for $V_{pol}(r)$ and $U_\ell(r)$ for s, p, d, and f orbitals in Mg$^+$ and Ca$^+$.

	Mg$^+$	Ca$^+$
α_d	0.48	3.254
α_q		6.936
$\alpha_q - 6\beta_1$	0.55	0.1
r_c	1.70	2.70
a_0^0	-3.12735685	-2.29441787
a_1^0	1.15200142	-2.52407057
a_2^0	0.00000010	0.76438518
a_3^0	1.60	1.69379665
a_0^1	-2.19519727	-2.76669788
a_1^1	0.60096237	-0.78422842
a_2^1	0.00013801	0.20964694
a_3^1	1.49926749	1.67437999
a_0^2	-4.08776863	-0.66418362
a_1^2	1.44385780	-3.00259360
a_2^2	-0.00028822	0.454
a_3^2	2.20216145	1.7
a_0^3	-0.17342163	-2.95458852
a_1^3	0.04784198	1.03975567
a_2^3	0.00078181	-0.08077417
a_3^3	1.40244082	1.32946388

they are included in Table I. The parameters for the potential $U_\ell(r)$ in Eq. (5) are obtained by adjusting our one-electron eigenvalues with respect to the first two or three experimental values in each ℓ symmetry [53], in a least-squares procedure. The process of minimization was performed using a Powell's algorithm of minimization without computing derivatives [54]. Our fitted parameters for the $U_\ell(r)$ potential are summarized in Table I for both Mg$^+$ and Ca$^+$, for s, p, d, and f orbitals. They are very similar to those reported in Ref. [27] for Mg$^+$. At variance, some differences appear for Ca$^+$, but it should be noted that the potential is optimized within a given functional space and we are using a reduced basis set of 22 B-splines. In fact, for a much larger B-spline basis set, our parameters for Ca$^+$ (more sensitive than Mg$^+$) become almost identical to those reported in Ref. [27] (which are computed with large Slater-type-orbital basis sets). Ours are also similar to the parameters of Table II in Hansen *et al.* [52].

In Table II we show in the case of Ca$^+$ how the one-electron energies are systematically improved after introducing the different components of the model potential; V_{HF}^d, $V_{HF}^d + V_{pol}$, and $V_{HF}^d + V_{pol} + U_\ell$. Separately, we have also calculated *ab initio* Hartree-Fock orbital energies (thus including exchange) corrected by a polarization potential as was done in Ref. [55] in terms of a similar B-spline basis and they are included also in Table II for Ca$^+$, quoted as V_{HF+pol}, for comparison. The polarization correction added to the Hartree-Fock direct potential $V_{HF}^d + V_{pol}$ provides minor

TABLE II. Energies (in a.u.) of [core]$n\ell$ states of Ca$^+$ ion. The values are referred to the Ca^{2+} core energy. Experimental energies are taken from NIST [53].

	V_{HF}^d	$V_{HF}^d + V_{pol}$	V_{HF+pol}	$V_{HF}^d + V_{pol} + U_l$	Expt.
$4s$	-0.36912090	-0.37678134	-0.44115755	-0.43627765	-0.43627765
$5s$	-0.17891810	-0.18089158	-0.19878977	-0.19858760	-0.19858760
$6s$	-0.10573311	-0.10653985	-0.11419224	-0.11424670	-0.11424670
$7s$	-0.06980039	-0.07021142	-0.07421396	-0.07425952	-0.07428465
$8s$	-0.04947032	-0.04970860	-0.05207946	-0.05209791	-0.05217450
$9s$	-0.03600937	-0.03619139	-0.03850457	-0.03799394	-0.03865600
$4p$	-0.27316876	-0.27741335	-0.32486866	-0.32081963	-0.32081963
$5p$	-0.14412748	-0.14550426	-0.16099691	-0.16023120	-0.16023120
$6p$	-0.08929698	-0.08992417	-0.09704760	-0.09678748	-0.09678748
$3d$	-0.24032747	-0.24773427	-0.37021958	-0.37528380	-0.37391690
$4d$	-0.13595959	-0.13833223	-0.17569313	-0.17739220	-0.17724645
$5d$	-0.08634585	-0.08738798	-0.10413107	-0.10517198	-0.10490701
$6d$	-0.05943461	-0.05998538	-0.06893807	-0.06956368	-0.06939455
$7d$	-0.04325195	-0.04358648	-0.04897722	-0.04937176	-0.04928392
$8d$	-0.03113345	-0.03143431	-0.03652622	-0.03620150	-0.03681006
$9d$	-0.01684593	-0.01719256	-0.02824038	-0.02311312	-0.02853735
$4f$	-0.12510496	-0.12599387	-0.12572934	-0.12618755	-0.12618755
$5f$	-0.08007907	-0.08056181	-0.08046160	-0.08072680	-0.08072680
$6f$	-0.05560988	-0.05589686	-0.05584862	-0.05601465	-0.05601465
$7f$	-0.04073983	-0.04093030	-0.04100051	-0.04101625	-0.04112010
$8f$	-0.02908951	-0.02928189	-0.03133223	-0.03137431	-0.03145950
$9f$	-0.01498478	-0.01522289	-0.02461846	-0.02464657	-0.02484065

TABLE III. $\ell_1\ell_2\ell_3$ type and number of configurations used to calculate resonances and photodetachment of Mg$^-$ and Ca$^-$ $^4P^e$. $\ell_1\ell_2\ell_3$-type configurations are indicated as $n_1,n_2,n_3\ell_1\ell_2\ell_3$, and N is the number of configurations for every $\ell_1\ell_2\ell_3$ type of configuration. n_i represents the number for the highest orbital included for the angular momentum ℓ_i.

$^4P^e$	N	$^4P^o$	N	$^4D^o$	N	$^4S^o$	N
				Mg$^-$			
$17,17,18spp$	2040	$17,17,18ssp$	2040	$17,14,18spd$	3510	$18,18,18ppp$	969
$15,17,18sdd$	1989	$17,18,14spd$	3584	$17,18,13sdf$	3510	$17,18,18pdd$	2736
$15,17,18sff$	1989	$12,17,18sdf$	3060	$7,18,17ppp$	1186	$17,18,18pff$	2736
$4,17,18ppd$	1566	$2,12,17ppp$	310	$14,18,4ppf$	1092	$14,18,18ddf$	2898
$3,17,18pdf$	1224	$2,12,17ppf$	170				
$1,17,18ddd$	475	$2,12,17ddp$	210				
Total	9283		9374		9298		9339
				Ca$^-$			
$17,18,18spp$	1904	$17,17,18ssp$	1456	$17,16,18spd$	3528	$18,18,18ppp$	816
$15,17,18sdd$	1836	$17,18,17spd$	3825	$17,18,14sdf$	3528	$18,18,18pdd$	2736
$15,17,18sff$	1836	$13,17,18sdf$	3060	$8,17,18ppp$	1024	$18,18,18pff$	2736
$6,17,18ppd$	1872	$4,12,17ppp$	491	$14,18,5ppf$	1200	$15,18,18ddf$	2970
$4,17,18pdf$	1224	$3,12,17ppf$	153				
$1,17,18ddd$	475	$3,12,17ddp$	210				
Total	9147		9195		9280		9258

changes and one may infer from these tables that the exchange correction is rather important. As mentioned previously, we were tempted to add to the direct Hartree-Fock potential a local approximation to the exchange potential. Doing this, we obtained energies similar to the *ab initio* Hartree-Fock orbital energies, but this option was finally excluded when we used U_ℓ, which is able to provide also the exchange interaction. Despite having reasonably good *ab initio* Hartree-Fock orbital energies coming from the $V_{\text{HF+pol}}$ potential, we finally realize that they are not good enough to provide correct threshold energy positions and resonance positions when the three-electron computations are performed, mainly for Ca$^-$, and high-precision orbitals obtained with the U_ℓ potential were finally required.

Ca$^+$, Ca, and Ca$^-$ are complicated atomic systems that are hard to compute accurately. It has already been pointed out that Ca I states with a pronounced $3d$ character in the configurations require an extra treatment. The $3d$ orbital has an appreciable overlap with the core, so that the interaction $3d$-core cannot be fully described with a core model potential. Furthermore, this core-valence interaction is term dependent in Ca [56]. To partially cure this problem, configurations containing d orbitals are improved by using a particular $U_{\ell=2}$ potential [29,52], which allows to reproduce the series $nd\ ^2D$ in Ca$^+$ with the supplementary constraint of matching the experimental value for the $3d^2\ ^3F$ term in Ca I (which has been measured without ambiguity). Of course, it is expected that a $U_{\ell=2}$ potential optimized for such a Ca I term does not provide perfect agreement for $nd\ ^2D$ in Ca$^+$ and for other Ca I terms containing d orbitals. In this sense, this choice is an approximation, but it improves things a lot. Then, for Ca$^+$, we have used the parameters for $U_{\ell=2}$ given in Ref. [52] and quoted in Table I for d orbitals. This d correction turns out to be crucial also for multiply excited states in Ca$^-$.

For each three-electron L, S, and π symmetry, we build three-electron $n\ell n'\ell'n''\ell''$-type configurations from the previous set of optimized s, p, d, and f orbitals, excluding $1s$, $2s$, and $2p$ core orbitals in Mg$^-$ and $1s$, $2s$, $2p$, $3s$, and $3p$ in Ca$^-$. The type and number of configurations used for $^4P^e$, $^4P^o$, $^4D^o$, and $^4S^o$ symmetries are included in Table III. The maximum number of configurations is always kept less than 10 000 to fit our computational resources. It is worth noting that the CSCI Hamiltonian matrix is dense and complex-symmetric and we are required to compute the whole set of eigenvalues and eigenfunctions to introduce them into the photodetachment cross section formula Eq. (9). Note also that for Ca$^-$ the number of configurations is reduced compared to Mg$^-$ since the number of one-electron orbitals is the same in both cases but the M-shell orbitals $3s$ and $3p$ are excluded from the CI expansion in the Ca$^-$ ion.

With this selection of configurations (including continuum orbitals), the Mg and Ca target states (all target thresholds listed in Table IV and Table VI) should be appropriately represented, along with the scattering channels. For example, the Mg [core]$3sn'p\ ^3P^o$ and Mg [core]$3pn's\ ^3P^o$ thresholds plus ϵs, ϵp, or ϵd escaping electrons, are accounted for with spp-type configurations from the $^4P^e$ symmetry, and ssp and spd from the $^4P^o$ symmetry, and spd from the $^4D^o$. We must remark that in our method the Mg I and Ca I threshold energies are obtained directly from the complex scaling diagonalization of the Mg$^-$ or Ca$^-$ problem. In other approaches, like the R-matrix method, the Mg I or Ca I target states are calculated previously as accurately as possible and afterward the channels Mg (or Ca)$+\epsilon(n\ell)$ are explicitly constructed. If not accurate enough, diagonal elements in the Hamiltonian matrix may be adjusted to reproduce the target experimental energies.

The initial state Mg$^-$ [core]$3s3p^2\ ^4P^e$ is computed with 9283 configurations and the energy obtained is

TABLE IV. Thresholds of the Mg$^-$ system. The experimental values are taken from NIST [53] relative to our theoretical EA value 0.364 08 eV. Energies are then given in eV and relative to the Mg$^-$([core]$3s3p^2\,{}^4P^e$) initial state.

State	Expt.	This work	Ref. [21]
Mg([core]$3s3p\,{}^3P^o$)	0.36408	0.36408	0.393
Mg([core]$3s4s\,{}^3S$)	2.75778	2.75880	2.824
Mg([core]$3s4p\,{}^3P^o$)	3.58233	3.59324	3.597
Mg([core]$3s3d\,{}^3D$)	3.59587	3.61775	3.624
Mg([core]$3s5s\,{}^3S$)	4.08133	4.10479	
Mg([core]$3s4d\,{}^3D$)	4.36894	4.36452	
Mg([core]$3s5p\,{}^3P^o$)	4.37628	4.38018	
Mg([core]$3s4f\,{}^3F^o$)	4.42901	4.42360	
Mg([core]$3p^2\,{}^3P$)	4.82289	4.81984	
Limit Mg II($^2S^e$)	5.29619		
Mg (core Thres I)	8.00589	8.03452	
Mg (core Thres II)		8.79945	
Mg (core Thres III)		9.15049	
Limit Mg II($^2P^o$)	9.71861		

$E = -0.747\,476\,947$ a.u. with respect to the Mg^{2+} core energy. For Mg$^-$ only the dipole correction to the $1/r_{12}$ interaction is included. We check the quality of our three-electron computation with our estimation of the electron affinities (EAs) of Mg I for its excited states. The EA for Mg $3s3p\,{}^3P^o$, i.e., $E(\mathrm{Mg}\,3s3p\,{}^3P^o) - E(\mathrm{Mg}^-\,3s3p^2\,{}^4P^e)$, is obtained in our three-electron calculation by extrapolating the lowest-energy continuum cut (Mg $3s3p\,{}^3P^o$ plus an escaping electron p within the total symmetry $^4P^e$) to the real axis, so that the electron excess energy is exactly zero. Our value for the EA (Mg $3s3p\,{}^3P^o$) is then 364 meV, to be compared with the theoretical values 367 meV [57] (with a relativistic HF-CI method), 379 meV [58] (with a multiconfiguration HF (MCHF) method), and 393.0 meV [21] (with a CI+R-matrix method). Note that we use the conversion factor 1 a.u. $= 27.211\,383\,44(M)/(M + m_e) = 27.210\,781\,8$ eV for Mg and all previous theoretical values have been then adapted. Similarly, our EA for the Mg $3p^2\,{}^3P^e$, $E(\mathrm{Mg}\,3p^2\,{}^3P) - E(\mathrm{Mg}^-\,3p^3\,{}^4P^e)$, is 545 meV, close to other theoretical values: 542 [57], 552 [58], and 541 [59]. The last work employs a three-electron B-spline CI result for Mg$^-$ and a separate two-electron B-spline CI result for Mg, with a core model potential developed by Aymar [33], less accurate than the one reported by Laughlin [27]. Unfortunately, experiments have not been successful in reporting EA values in Mg [60]. We compare some of our theoretical thresholds with experimental ones from the NIST database [53] in Table IV, taking our EA as reference. Our Mg I threshold positions are in good accordance with the NIST values below the Mg$^+$ ($^2S^e$) threshold. We follow the labels given by NIST below the Mg$^+$ ($^2S^e$) limit, but we were unable to identify labels above the first double continuum threshold, either in theory or experiment.

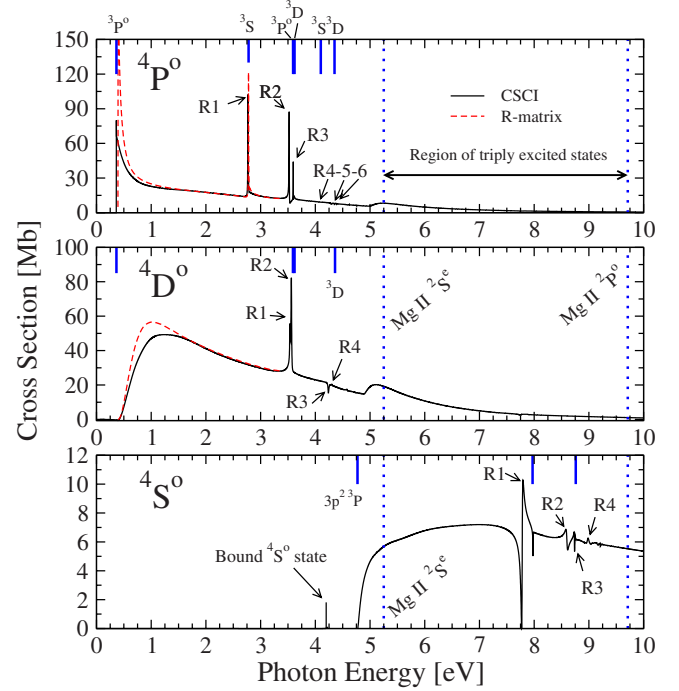Our CSCI method implicitly includes all contributions coming from partial channels because of the way we con-

FIG. 2. (Color online) Calculated partial photodetachment cross section to Mg$^-$ $^4P^o$, $^4D^o$, and $^4S^o$ final symmetries from the metastable Mg$^-$ [core]$3s3p^2\,{}^4P^e$ state. (Black) solid line, our CSCI result with a rotation angle $\theta = 15°$; (red) dashed line, R-matrix result by Zeng *et al.* [21]. The vertical (blue) thick lines indicate our Mg I thresholds [core]$n\ell n'\ell'\,{}^3L^\pi$ quoted in Table IV; the vertical long thick dotted lines indicate the positions of the Mg II double-ionization thresholds $^2S^e$ and $^2P^o$, enclosing a region of triply excited states. Resonance positions are labeled as Rn and the arrows point to the maximum cross sections of the CSCI calculation.

struct the three-electron configurations (see Table III). For instance, for Mg$^-$ $^4P^o$ symmetry, the ssp and spd configurations allow us to account for channels [$3s3p\,{}^3P^o + (\epsilon s, \epsilon d)$], [$3s4s\,{}^3S + \epsilon p$], [$3s4p\,{}^3P^o + (\epsilon s, \epsilon d)$], [$3s3d\,{}^3D + \epsilon p$], and so on. Unfortunately, complex scaling cannot separate contributions to cross sections and widths associated with individual channels within a given total angular symmetry. We provide instead the whole contribution to the cross section coming from each final angular symmetry, which we call here partial cross sections. In Fig. 2 we plot the partial photodetachment cross sections to the final states $^4P^o$, $^4D^o$, and $^4S^o$ with photon energy from 0 to 10 eV. We have been able to identify up to 14 resonant states, six $^4P^o$, four $^4D^o$, and four $^4S^o$, at variance with the only previous R-matrix computation [21], which reported only the first $^4P^o$ resonance. Our resonance parameters (positions, widths, and Fano q parameters) are summarized in Table V. The q shape parameter is obtained with CSCI following the same procedure given in Ref. [25]. Not all resonances produce noticeable features in the photodetachment spectra. We clarify the true resonant nature of the peaks by exploring the behavior of the eigenvalues in the complex plane. Those eigenvalues unaffected after different rotation angles are assigned to S-matrix poles. Therefore each resonance Rn quoted in the photodetachment spectrum in Fig. 2 has its counterpart in the complex plane, as indicated in Fig. 3.

TABLE V. Mg$^{-4}P^o$, $^4D^o$, and $^4S^o$ resonance parameters in the photon energy region 0–10 eV. E_r is the binding energy in a.u. relative to the ground state of the Mg^{2+} core, while the position in eV is relative to the Mg$^-$([core]$3s3p^{2\ 4}P^e$) initial state.

| Resonance	E_r (a.u.)	$-\Gamma/2$ (a.u.)	Position (eV)	Width (meV)	q
		$^4P^o$			
$R1$	-0.6463148	-1.367×10^{-4}	2.7527	7.44	31.9
$R2$	-0.6185508	-1.088×10^{-4}	3.5082	5.92	-4.77
$R3$	-0.6154984	-2.527×10^{-4}	3.5912	13.75	-5.06
$R4$	-0.5972059	-1.376×10^{-3}	4.0889	2.43	0.053
$R5$	-0.5904219	-5.600×10^{-4}	4.2735	30.48	-0.036
$R6$	-0.5882176	-2.142×10^{-4}	4.3336	11.66	-0.021
		$^4D^o$			
$R1$	-0.6158453	-1.232×10^{-4}	3.5818	6.70	-6.29
$R2$	-0.6155770	-1.823×10^{-4}	3.5891	9.92	-59.9
$R3$	-0.5888939	-4.142×10^{-4}	4.3151	22.54	-0.116
$R4$	-0.5872205	-1.223×10^{-5}	4.3607	6.66	-0.380
		$^4S^o$			
$R1$	-0.4596686	-4.480×10^{-4}	7.8315	24.38	0.694
$R2$	-0.4297287	-6.147×10^{-4}	8.6461	33.45	-0.891
$R3$	-0.4247147	-1.188×10^{-4}	8.7826	6.47	-0.377
$R4$	-0.4156619	-4.139×10^{-4}	9.0289	22.52	4.925
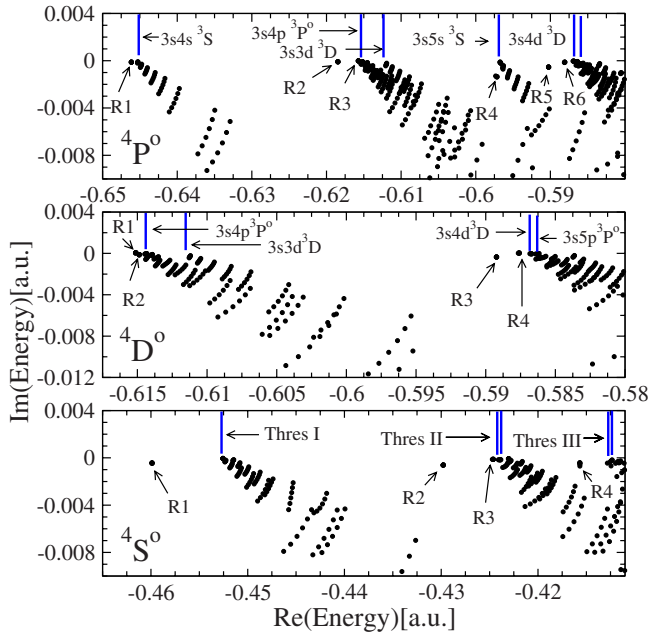
FIG. 3. (Color online) Complex eigenvalue spectrum of Mg$^-$ $^4P^o$, $^4D^o$, and $^4S^o$ symmetries for different values of the rotation angles from $\theta = 10°$ to $20°$. The eigenvalues fall into the lower half of the complex plane with an angle 2θ. The eigenvalues accumulated at fixed points—not affected by the complex rotation—show a resonance behavior and they are labeled as Rn. (Blue) vertical lines indicate the position of our Mg I thresholds [core]$nln'l'$ $^3L^\pi$ included in Table IV.

In Fig. 2 we have also included R-matrix results up to the limit 0.25 Ry (~3.4 eV) as published in Ref. [21]. For the nonresonant background cross section, our $^4P^o$ and $^4D^o$ results agree in general (except just above the Mg $3s3p$ $^3P^o$ threshold) with the R-matrix result. The only resonance reported in Ref. [21], $^4P^o$ at 0.2 Ry (~2.7 eV), compares with our $^4P^o$ $R1$ resonance at 2.75 eV. Minor differences in positions are due to the different accuracy in the computations of Mg I thresholds. Above the first Mg$^+$ threshold at ~5.25 eV, R-matrix methods cannot be applied since *two electrons* are ejected. Indeed, additional R-matrix strong peaks appearing at ~5.25 eV (Mg$^+$ threshold) along with others at higher photon energies are only artifacts in the R-matrix computation [61]. Conversely, in our CSCI approach, double-ionization continua are included and well described and this allows us to report the cross section between the first and the second double-ionization thresholds. This means that triply excited states are reached by photon absorption and they decay generally into autoionizing doubly excited states of Mg I. The symmetry $^4S^o$, not calculated in Ref. [21], is responsible for the major features between Mg$^+$ $^2S^e$ and Mg$^+$ $^2P^o$ thresholds, and the cross section is dominated by the Feshbach resonance $^4S^o$, $R1$.

At this point, although some calculations for doubly excited states in Mg are available [62,63], we were not able to clearly identify the labels corresponding to the Mg thresholds (doubly excited states) appearing in the complex energy plane for $^4S^o$ symmetry, and only the energy positions are indicated. In Fig. 6 below we plot our Mg$^-$ total photodetachment cross section and compared to the R-matrix result. In conclusion, apart from a slight difference in the back-

ground from 0.5 to 1.5 eV we confirm the R-matrix result published up to 3.4 eV. The most noticeable features in the photodetachment spectra are now revealed from 0 to 10 eV and any potential future experiment should be able to locate a strong peak at ~ 2.7 eV, several overlapping peaks at ~ 3.6 eV, and a noticeable signature from a triply excited state that comes from the $^4S^o$ symmetry at ~ 7.8 eV.

The initial state Ca$^-$ [core]$4s4p^2\,^4P^e$, first predicted as a bound metastable state by Bunge [7], is computed with 9147 configurations with a corresponding energy $E = -0.614\,86$ 9176 a.u. with respect to the Ca^{2+} core energy. Again, in order to assess our computation we obtain an EA for Ca I $4s4p\,^3P^o$ state through the energy difference $E(\text{Ca }4s4p\,^3P^o)$ $-E(\text{Ca}^-\,4s4p^2\,^4P^e)$. Here we use a conversion factor for Ca 1 a.u.$=27.211\,011\,0$ eV. The threshold energy for Ca $4s4p\,^3P^o$ may be obtained from different symmetries (for instance $^4P^e$ or $^4P^o$) by extrapolating the continuum cuts to the zero axis. We get 515.68 meV from $^4P^e$ and 517.58 meV from $^4P^o$, so that our method has an uncertainty of ~ 2 meV. This values may be compared to 515.8 meV [37], obtained by separately computing Ca $4s4p\,^3P^o$ and Ca$^-\,4s4p^2\,^4P^e$ with a two- and a three-electron code, respectively, based on B-splines and including the dielectronic polarization potential. We use basically an identical method (but complex-rotated) and a rather good comparison is expected, although we stress again that with our method it is more demanding to obtain the Ca threshold energies since they are obtained at the same three-electron run. Since other precise computations (namely, 517 ± 10 meV with a MCHF calculation from [37] and 512 meV from [64]) also agree with our value, it seems that the theoretical binding energy of Ca$^-\,^4P^e$ is by now a settled matter. The EA reported by Zeng *et al.* [21] is 559.5 meV, close to the value when dielectric core polarization terms are excluded. At the time of publication of Ref. [37], the experimental binding energy available [11] was 555 ± 5. Later on, Kristensen *et al.* [13] introduced a new state-selective depletion spectroscopy that allowed measurement of the binding energy with high accuracy, providing an EA value of 521.84 eV, thus supporting the most sophisticated calculations.

In Ca$^-$, our CSCI Ca I thresholds are compared with experimental ones from the NIST database [53] in Table VI, using the experimental EA of Ref. [13]. Our Ca threshold positions becomes systematically shifted upward ~ 0.1–0.2 eV in energy. In the R-matrix computation for Ca$^-$ [21], Ca thresholds were obtained more accurately by using optimized HF orbitals in fitting the energy levels of atomic Ca and then supplemented with $3p$ core excitations to partially account for core-valence correlations. We expect a loss of accuracy in our Ca thresholds due to the high number of three-electron configurations required, in contrast with a direct Ca two-electron CI computation. Unfortunately we could not afford larger CI expansions with our computational resources.

In Ca$^-$, the set of configurations given in Table III allows for the description of the different partial channels within the photon energy region considered. For example, the lowest ionization channels within the final $^4P^o$ symmetry, namely, $[4s4p\,^3P^o + (\epsilon s, \epsilon d)]$ are accounted for with ssp and spd configurations, channels $[3d4s\,^3D + (\epsilon p, \epsilon f)]$ with spd and sdf

TABLE VI. Thresholds of the Ca$^-$ system. The experimental values are taken from NIST [53]. Energies are given in eV and relative to the Ca$^-$([core]$4s4p^2\,^4P^e$) initial state.

State	Expt.	This work	Ref. [21]
Ca([core]$4s4p\,^3P^o$)	0.52184	0.51568	0.5595
Ca([core]$3d4s\,^3D$)	1.15336	1.27949	1.176
Ca([core]$4s5s\,^3S$)	2.53986	2.57085	2.529
Ca([core]$3d4p\,^3F^o$)	3.07196	3.20696	3.092
Ca([core]$4s5p\,^3P^o$)	3.16297	3.26573	
Ca([core]$4s4d\,^3D$)	3.31032	3.37520	
Ca([core]$3d4p\,^3D^o$)	3.36968	3.46954	3.470
Ca([core]$4p^2\,^3P$)	3.43697	3.50906	3.485
Ca([core]$3d^2\,^3F$)	4.02201	4.11308	
Ca([core]$3d^2\,^3P$)	4.64895	4.70628	
Limit Ca II($^2S_{1/2e}$)	4.74262		
Ca([core]$3d5p\,^3D^o$)	5.04498	5.11020	
Limit Ca II($^2D_{3/2}$)	6.43503		
Limit Ca II($^2D_{5/2}$)	6.44255		
Limit Ca II($^2P_{1/2}$)	7.86597		

configurations, channels $[4s5s\,^3S + (\epsilon p)]$ with the ssp ones, and $[3d4p\,^3F^o + (\epsilon d)]$ with the ddp ones. A similar analysis may be performed for the ionization channels in $^4D^o$ and $^4S^o$ final symmetries. The partial photodetachment cross sections to the final states $^4P^o$, $^4D^o$, and $^4S^o$ as a function of the photon energy are given in Fig. 4. Three different results are displayed. Our most accurate result is obtained with the use of the model potential in Eq. (2) and the dielectronic interaction from Eq. (8) and applying complex scaling (calculation type A). We compare with the R-matrix result from Ref. [21] and also with the result we obtain by using Ca$^+$ Hartree-Fock orbitals (plus a polarization potential) whose orbital energies are given in Table II in the column labeled $V_{\text{HF+pol}}$ (called hereafter calculation type B). In the latter type B calculation we do not include any dielectronic polarization correction or any extra *special treatment* for the d orbitals.

A pronounced broad $^4P^o$ Feshbach resonance (denoted $R1$ in Fig. 4) is located slightly below the Ca I $3d4s\,^3D$ threshold, and also two small sharp Feshbach resonances ($R2$ and $R3$) just below the Ca I $4s5s\,^3S$ and the Ca I $3d4p\,^3F^o$ thresholds, respectively. Both of our CSCI calculations (types A and B) uncover these three resonance peaks but they differ noticeably in the positions, in fact, due to the distinct Ca threshold positions resulting from the two calculations. Our calculation type A produces a much better matching with the experimental Ca I thresholds and gets closer to the R-matrix result for the $R1$ resonance as well. It happens similarly with the other $^4P^o$ $R2$ and $R3$ resonances. The corrections for the Ca I thresholds in the $^4P^o$ symmetry are better illustrated by inspecting the complex eigenvalue spectrum in Fig. 5. The vertical lines in Fig. 5 in the region Im$(E) > 0$ indicate Ca I thresholds for our two different CSCI calculations. The upper ones (in blue) correspond to the calculation type B (HF) and the lower ones (in black) show how these threshold positions
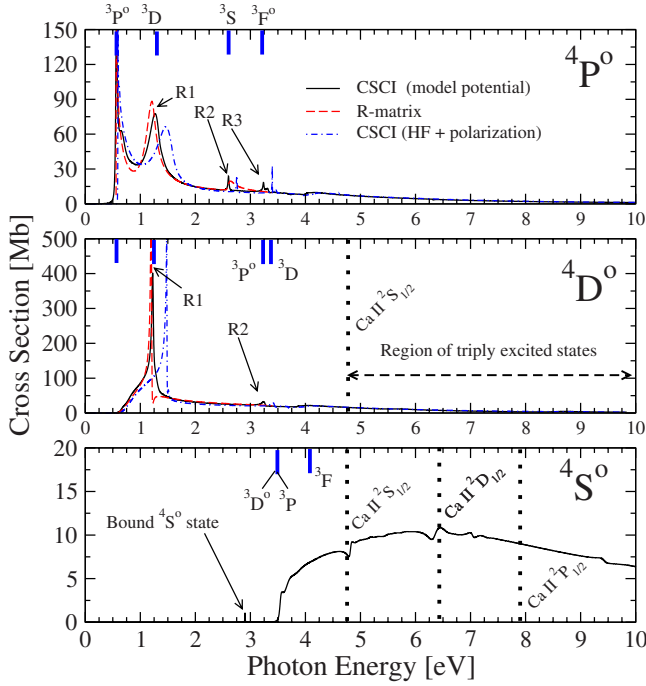
FIG. 4. (Color online) Calculated partial photodetachment cross section to Ca$^-$ $^4P^o$, $^4D^o$, and $^4S^o$ final symmetries from the metastable Ca$^-$ [core]$4s4p^2$ $^4P^e$ state. (Black) solid line, our CSCI result type A with a rotation angle $\theta = 15°$ (blue) dash-dotted line, our CSCI result type B with $\theta = 15°$; (red) dashed line, R-matrix result by Zeng *et al.* [21]. The vertical (blue) thick lines indicate Ca I thresholds [core]$n\ell n'\ell'$ $^3L^\pi$ taken from the NIST database quoted in Table VI; the vertical long thick dotted lines indicate the positions of the Ca II double-ionization thresholds. Resonance positions are labeled as Rn and the arrows point to the maximum cross section of the CSCI calculation.

become corrected in the calculation type A (model potential). It is the joint correction for Ca $4s4p$ $^3P^o$ and Ca $3d4s$ ^3D thresholds that improves the position of the $R1$ resonance with respect to the Ca I $4s4p$ $^3P^o$ threshold. It should be kept in mind that the energy for the initial $^4P^e$ state is also different in the A and B calculations. We then conclude that the corrections included in the type A calculation are indeed very important to produce a correct photodetachment spectrum. Our $^4P^o$ result of type A now compares quite well with the
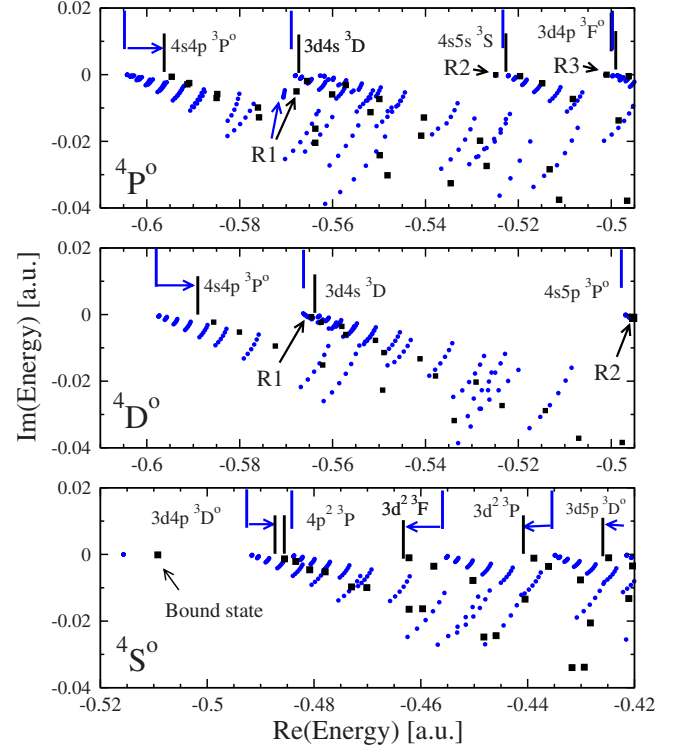

FIG. 5. (Color online) Complex eigenvalue spectrum of Ca$^-$ $^4P^o$, $^4D^o$, and $^4S^o$ symmetries. (Black) squares, CSCI result type A for a rotation angle $\theta = 15°$; (blue) circles, CSCI result type B for six different values of the rotation angle from $\theta = 10°$ to $20°$. Vertical lines indicate the position of our Ca I thresholds [core]$n\ell n'\ell'^3L^\pi$. Upper thresholds (in blue) correspond to a calculation type B and lower thresholds (in black) to the model potential calculation type A (see text for further explanation). The latter are those quoted in Table VI.

R-matrix result up to ~ 3.2 eV. Additionally, $^4P^o$ $R2$ and $R3$ resonances were not predicted by the R-matrix computation, which shows instead only a small bump at ~ 2.6 eV corresponding to the opening of the threshold.

We can now proceed with a similar analysis for the $^4D^o$ final symmetry. Unfortunately, our calculation for the final $^4D^o$ symmetry is not as good as for the other symmetries and eventually it should require many more configurations. This is reflected in Fig. 5, in comparing the positions of the first

TABLE VII. Ca$^-$$^4P^o$, $^4D^o$, and $^4S^o$ resonance parameters in the photon energy region $0-10$ eV. E_r is the binding energy in a.u. relative to the ground state of Ca^{2+} core, while the position in eV is relative to the Ca$^-$([core]$4s4p^2$ $^4P^e$) state.

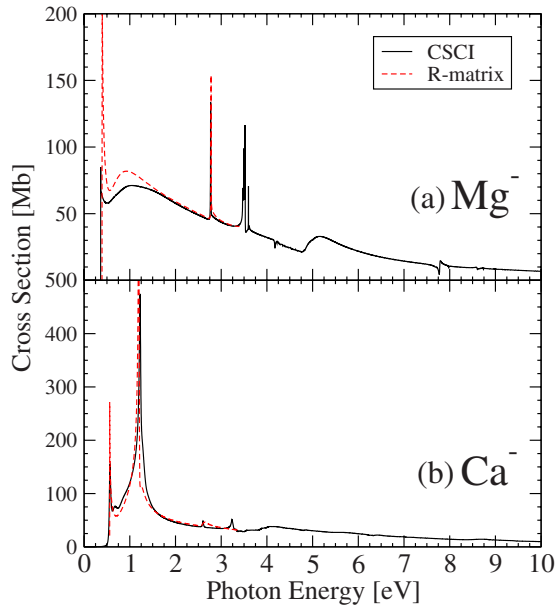| Resonance	E_r (a.u.)	$-\Gamma/2$ (a.u.)	Position (eV)	Width (meV)	q
		$^4P^o$			
$R1$	-0.5681385	-5.029×10^{-3}	1.2716	273.7	-8.95
$R2$	-0.5211942	-2.332×10^{-4}	2.5490	12.69	-10.5
$R3$	-0.4978136	-8.085×10^{-6}	3.1852	0.4399	-3.71
		$^4D^o$			
$R1$	-0.56814	-6.205×10^{-4}	1.272	33.77	-4.34
$R2$	-0.49462	-9.269×10^{-4}	3.272	50.44	-1.41

FIG. 6. (Color online) Total photodetachment cross section $(^4P^o+{}^4D^o+{}^4S^o)$ from the metastable Mg⁻ (a) and Ca⁻ (b) $^4P^e$ state. (Black) solid line, CSCI result; (red) dashed line, R-matrix result by Zeng *et al.* [21].

two Ca I thresholds $4s4p$ and $3d4s$ in both $^4P^o$ and $^4D^o$ symmetries. They are clearly misaligned with respect to each other, even with the calculation type A. Since the Ca⁻ $^4P^e$ initial state energy is the same, our option is to shift our $^4D^o$ photodetachment spectrum (types A and B) to fit the first Ca I $4s4p\,{}^3P^o$ threshold. Then the position of the first $^4D^o$ $R1$ strong Feshbach resonance should be located almost exactly at the same position as our first $^4P^o$, at 1.2716 eV. Including this shift, one may appreciate in Fig. 4 that the $^4D^o$ $R1$ resonance in the HF calculation type B is wrongly located at a higher energy ~ 1.5 eV, indicating again the necessity for the corrections provided by the model potential and the dielectronic polarization interaction. A second small $^4D^o$ $R2$ resonance is found between the $4s5p\,{}^3P^o$ and the $4s4d\,{}^3D$ thresholds at ~ 3.27 eV.

At variance with Mg⁻, the $^4S^o$ symmetry barely shows specific peaks in the photodetachment spectra, which is in principle quite unexpected. The small features are indeed due to threshold openings, since the complex eigenvalue spectrum does not show any signature of poles. It seems that the more complex nature of the Ca⁻ ion washes out any trace of triply excited states and probably this is a trend in heavier alkaline-earth negative ions. Our Ca⁻ resonance parameters (positions, widths, and q parameters) for the quartets are summarized in Table VII. Note that in this table the resonance positions for $^4D^o$ were corrected according to our

thresholds for the $^4P^o$ symmetry quoted in Table VI.

Finally, in Fig. 6 we plot our Ca⁻ total photodetachment cross section. Our comparison with the R-matrix result up to ~ 3.2 eV is good. In contrast to Mg⁻, and surprisingly to us, we add little to the known R-matrix result, which already gives the main noticeable structures in the total spectrum. At least, our study of Ca⁻ reveals how important it is to introduce high-level corrections due to the presence of a complex polarizable core in order to achieve accurate results in its photoionization spectra.

IV. CONCLUSION

A complex scaled configuration interaction approach, based on the use of B-spline basis sets combined with a sophisticated core model potential (mono- and dielectronic polarization effects) has been used to compute the photodetachment cross sections of $^4P^e$ states of Mg⁻ and Ca⁻ negative ions. Our CSCI results confirm and notably extend the R-matrix results given in Ref. [21]. Up to 14 resonances are reported in Mg⁻ and five in Ca⁻. Mg⁻ is still a quite unexplored ion due to its elusive stability and Ca⁻ has a very confusing experimental history as mentioned in the Introduction. We hope our results can stimulate new high-precision measurements on the photodetachment of these negative ions to be carried out, at least in the energy region where resonances are now predicted.

This paper sheds light on the presence or absence of resonant doubly and triply excited states in Mg⁻ and Ca⁻ ions, and it provides important theoretical input into the photodetachment of these two controversial negative ions. In spite of using the best state of the art tools to compute the photodetachment of Ca⁻, this ion still reveals itself as one of the most complicate systems to compute with spectroscopic accuracy. To go beyond Ca⁻ in the alkaline-earth series would require explicit relativistic corrections in our approach. Our methodology also could be suitable to explore the photodynamics of triply excited states subject to strong ultrashort laser pulses by implementing a time-dependent propagation, either within the complex scaling scheme or with a time-dependent Feshbach-like approach. Steps along those directions are under our present consideration.

[1] G. J. Schulz, Rev. Mod. Phys. **45**, 378 (1973).

[2] H. S. W. Massey, *Negative Ions*, 3rd ed. (Cambridge University Press, Cambridge, U.K., 1976).

[3] H. S. W. Massey, Adv. At. Mol. Phys. **15**, 1 (1979).

[4] S. J. Buckman and C. W. Clark, Rev. Mod. Phys. **66**, 539 (1994).

[5] T. Andersen, Phys. Rep. **394**, 157 (2004).

[6] D. J. Pegg, Rep. Prog. Phys. **67**, 857 (2004).

[7] C. F. Bunge, M. Galán, R. Jáuregui, and A. V. Bunge, Nucl. Instrum. Methods Phys. Res. **202**, 299 (1982).

[8] Y. K. Bae and J. R. Peterson, Phys. Rev. A **30**, 2145 (1984).

[9] T. J. Kvale, G. D. Alton, R. N. Compton, D. J. Pegg, and J. S. Thompson, Phys. Rev. Lett. **55**, 484 (1985).

[10] J. O. Gaardsted and T. Andersen, J. Phys. B **22**, L51 (1989).

[11] D. Hanstorp, P. Devynck, W. G. Graham, and J. R. Peterson, Phys. Rev. Lett. **63**, 368 (1989).

[12] V. V. Petrunin, H. H. Andersen, P. Balling, and T. Andersen, Phys. Rev. Lett. **76**, 744 (1996).

[13] P. Kristensen, C. A. Brodie, U. V. Pedersen, V. V. Petrunin, and T. Andersen, Phys. Rev. Lett. **78**, 2329 (1997).

[14] G. F. Gribakin, B. V. Gul'tsev, V. K. Ivanov, and M. Yu. Kuchiev, J. Phys. B **23**, 4505 (1990).

[15] C. Froese Fischer and J. E. Hansen, Phys. Rev. A **44**, 1559 (1991).

[16] V. K. Ivanov, in *Correlations in Clusters and Related Systems: New Perspectives on the Many-Body Problem*, edited by J.-P Connerade (World Scientific, Singapore, 1993).

[17] J. Yuan and L. Fritsche, Phys. Rev. A **55**, 1020 (1997); J. Yuan, *ibid.* **61**, 012704 (1999).

[18] E. Heinicke, H. J. Kaiser, R. Rackwits, and D. Feldmann, Phys. Lett. A **50**, 265 (1974).

[19] C. W. Walter and J. R. Peterson, Phys. Rev. Lett. **68**, 2281 (1992); J. R. Peterson, Aust. J. Phys. **40**, 293 (1992).

[20] D. H. Lee, D. J. Pegg, and D. Hanstorp, Phys. Rev. A **58**, 2121 (1998); D. H. Lee, M. B. Poston, D. J. Pegg, D. Hanstorp, and U. Berzinsh, *ibid.* **60**, 715 (1999).

[21] J. Zeng, J. Yuan, and Q. Lu, Phys. Rev. A **62**, 022713 (2000).

[22] J. L. Sanz-Vicario and E. Lindroth, Phys. Rev. A **68**, 012702 (2003).

[23] A. Hibbert, Adv. At. Mol. Phys. **18**, 309 (1982).

[24] C. Laughlin and G. A. Victor, Adv. At. Mol. Phys. **25**, 163 (1989).

[25] J. L. Sanz-Vicario and E. Lindroth, Phys. Rev. A **65**, 060703(R) (2002); J. L. Sanz-Vicario, E. Lindroth, and N. Brandefelt, *ibid.* **66**, 052713 (2002).

[26] E. Lindroth and J. L. Sanz-Vicario, Radiat. Phys. Chem. **70**, 387 (2004).

[27] C. Laughlin, Phys. Scr. **45**, 238 (1992).

[28] C. Laughlin, J. Phys. B **28**, 2787 (1995).

[29] C. Laughlin and J. E. Hansen, J. Phys. B **29**, L441 (1996).

[30] H. W. van der Hart, C. Laughlin, and J. E. Hansen, Phys. Rev. Lett. **71**, 1506 (1993).

[31] H. Bachau, E. Cormier, P. Decleva, J. E. Hansen, and F. Mar-

tín, Rep. Prog. Phys. **64**, 1815 (2001).

[32] B. J. Albright, K. Bartschat, and P. R. Flicek, J. Phys. B **26**, 337 (1993).

[33] M. Aymar, C. H. Greene, and E. Luc-Koening, Rev. Mod. Phys. **68**, 1015 (1996).

[34] R. Santra, K. V. Christ, and C. H. Greene, Phys. Rev. A **69**, 042510 (2004).

[35] H. W. van der Hart, Ph.D. thesis, University of Amsterdam, 1994.

[36] C. Froese Fischer and T. Brage, Can. J. Phys. **71**, 1283 (1993).

[37] C. F. Fischer, J. E. Hansen, and H. W. van der Hart, Phys. Rev. A **51**, 1999 (1995).

[38] E. Clementi and C. Roetti, At. Data Nucl. Data Tables **14**, 177 (1974).

[39] J. B. Furness and I. E. McCarthy, J. Phys. B **6**, 2280 (1973).

[40] C. W. McCurdy, M. Baertschy, and T. N. Rescigno, J. Phys. B **37**, R137 (2004).

[41] B. Simon, Phys. Lett. **71A**, 211 (1979).

[42] W. Reinhardt, Annu. Rev. Phys. Chem. **33**, 223 (1982).

[43] C. W. McCurdy, in *Autoionization: Recent Developments and Applications*, edited by A. Temkin (Plenum Press, New York 1985).

[44] C. H. Maier, L. S. Cederbaum, and W. Domcke, J. Phys. B **13**, L119 (1980).

[45] C. W. McCurdy and F. Martín, J. Phys. B **37**, 917 (2004).

[46] C. D. H. Chisholm and U. Öpik, Proc. Phys. Soc. London **83**, 541 (1964).

[47] G. Peach, in *Atoms in Astrophysics*, edited by P. G. Burke, W. B. Eissner, D. G. Hummer, and I. C. Percival (Plenum Press, New York, 1983).

[48] T. N. Rescigno and V. McKoy, Phys. Rev. A **12**, 522 (1975).

[49] I. B. Bersuker, Opt. Spektrosk. **3**, 97 (1957).

[50] S. Hameed, A. Herzenberg, and M. G. James, J. Phys. B **1**, 822 (1968).

[51] D Hafner and W. H. E. Schwarz, J. Phys. B **11**, 2975 (1978).

[52] J. E. Hansen, C. Laughlin, H. W. van der Hart, and G. Verbockhaven, J. Phys. B **32**, 2099 (1999).

[53] NIST Atomic Spectra DataBase, http://physics.nist.gov

[54] R. P. Brent, *Algorithms for Minimization without Derivatives* (Dover Publications, New York, 2002). M. J. D. Powell, Comput. J. **7**, 155 (1964).

[55] E. Lindroth, Phys. Rev. A **52**, 2737 (1995).

[56] C. Froese Fischer and J. E. Hansen, J. Phys. B **18**, 4031 (1985).

[57] D. R. Beck, Phys. Rev. A **40**, 2887 (1989).

[58] C. F. Fischer, Phys. Rev. A **41**, 3481 (1990).

[59] H. W. van der Hart, Phys. Rev. A **59**, 1125 (1999).

[60] T. Andersen, T. Brage, C. Froese-Fischer, and L. Eg Sorensen, J. Phys. B **24**, 905 (1991).

[61] J. Zeng, J. Yuan, and Q. Lu (private communication).

[62] R. Moccia and P. Spizzo, Phys. Rev. A **39**, 3855 (1989).

[63] T. K. Fang and T. N. Chang, Phys. Rev. A **61**, 052716 (2000).

[64] R. D. Cowan and M. Wilson, Phys. Scr. **43**, 244 (1991).